HHS Public Access

Author manuscript

Heart Rhythm. Author manuscript; available in PMC 2017 September 01.

Published in final edited form as:

Heart Rhythm. 2016 September ; 13(9): 1922–1931. doi:10.1016/j.hrthm.2016.05.017.

Mechanisms Linking Electrical Alternans and Clinical Ventricular Arrhythmia in Human Heart Failure

J.D. Bayer, PhD[a,b], **G.G. Lalani, MD**[c], **E.J. Vigmond, PhD**[a,b], **S.M. Narayan, MD, PhD, FHRS**[d], and **N.A. Trayanova, PhD, FHRS**[e]

[a]Electrophysiology and Heart Modeling Institute (LIRYC), Bordeaux University Foundation, France

[b]Institute of Mathematics of Bordeaux (U5251), University of Bordeaux, France

[c]University of California, San Diego, CA

[d]Stanford University, Palo Alto, CA

[e]Institute for Computational Medicine, Johns Hopkins University, Baltimore, MD

Abstract

Background—Mechanisms of ventricular tachycardia (VT) and fibrillation (VF) in heart failure (HF) patients are undefined.

Objective—Utilize a computational-clinical approach to elucidate VT/VF mechanisms in HF.

Methods—In 53 HF and 18 control patients, we established the relationship between low-amplitude action potential voltage alternans (APV-ALT) at near-resting heart-rates and VT/VF on long-term follow-up. Mechanisms underlying the transition of APV-ALT to VT/VF, which cannot be ascertained in patients, were dissected with multi-scale human ventricular models (HVM) based on human electrophysiological and MRI data (control and HF).

Results—For patients with APV-ALT k-scores>1.7, complex action potential duration (APD) oscillations (≥2.3% of mean APD), rather than APD alternans, most accurately predicted VT/VF during long-term follow-up (+82%; −90% predictive values). In the failing HVM, abnormal sarcoplasmic reticulum (SR) calcium handling caused APV-ALT (>1mV) during pacing with 550ms cycle length (CL), that transitioned into large magnitude (>100ms) discordant repolarization time alternans (RT-ALT) at faster rates. This initiated VT/VF (CL<400ms) by steepening apicobasal repolarization (189ms/mm) until unidirectional conduction block and reentry. Complex APD oscillations resulted from non-stationary discordant RT-ALT. Restoring SR calcium to control levels was antiarrhythmic by terminating electrical alternans.

Correspondence: Jason Bayer, LIRYC, Campus Xavier Arnozan, Avenue du Haut Lévêque, 33600 Pessac, France, Phone: +330535381955, jason.bayer@ihu-liryc.fr.

Disclosures:

Narayan: Topera Inc. equity; Medtronic speaker fees; American College of Cardiology Foundation consulting fees; UpToDate royalties.

Trayanova: CardioSolv LLC ownership.

Conclusions—APV-ALT and complex APD oscillations at near-resting heart-rates in HF patients are linked to arrhythmogenic discordant RT-ALT. This may enable novel physiologically-tailored, bioengineered indices to improve VT/VF risk stratification, where SR calcium handling and spatial apicobasal repolarization are potential therapeutic targets.

Keywords

alternans; arrhythmia; heart failure; computer modeling; simulation

Introduction

Emergence of low-amplitude action potential voltage alternans (APV-ALT) at near-resting heart-rates precedes life-threatening ventricular arrhythmias in heart failure (HF) patients[1]. APV-ALT during slow rates is the consequence of calcium transient (CaT) alternans (CaT-ALT), caused by abnormal sarcoplasmic reticulum (SR) calcium handling in HF[2]. However, the mechanisms linking APV-ALT in HF with arrhythmogenesis remain undefined.

Local repolarization time (RT) in the ventricles is activation time plus action potential duration (APD). In structurally-normal animal hearts, CaT-ALT at rapid pacing rates produces arrhythmogenic repolarization time alternans (RT-ALT), e.g. adjacent ventricular regions exhibiting RT-ALT 180° out of phase[3]. Discordant RT-ALT steepens repolarization gradients to promote unidirectional block and reentry[4], and is attributed to electrophysiological heterogeneities[3] and/or slowed conduction[5].

Patients with HF are at risk of ventricular tachycardia (VT) and fibrillation (VF). Notably, failing human hearts exhibit widely remodeled electrophysiological parameters[6,7] and conduction slowing[8]. This could produce detectable APV-ALT near-rest that transition into discordant RT-ALT to initiate VT/VF at faster rates. However, this is unestablished in the failing human ventricles, and is this research's hypothesis.

This hypothesis was tested using a computational-clinical approach. First, a clinical study established the relationship between APV-ALT and VT/VF outcome on long-term follow-up in HF patients. To determine the mechanisms of this transition, which cannot be ascertained *in vivo*, multi-scale computational human ventricles models (HVMs) were developed with human electrophysiological and MRI data. These HVMs, one without (control) and one with HF electrophysiology, were used to determine the i) pacing threshold and spatial distribution of APV-ALT and RT-ALT, ii) mechanistic relationship between APV-ALT, RT-ALT, and arrhythmogenesis, and iii) key components of electrophysiological remodeling and spatial heterogeneity underlying arrhythmogensis.

Methods

See Supplementary Table 1 for abbreviations.

Computational

HVMs—Anatomically accurate HVMs were derived from a high-resolution MRI scan of an adult human heart geometry and fiber orientation (Supplementary Section 2). They

simulated transmural and apicobasal electrophysiological heterogeneity in nonfailing and failing human ventricles. The failing HVM featured a reduced transmural APD gradient from epicardial APD prolongation[6], reduced amplitude and slow recovering CaT from deranged calcium handling[7], and slow conduction from fibrosis and/or reduced Cx43 expression[8]. These features make the HVM the most complete model of human ventricular electrophysiology to date (Supplementary Sections 2–6).

Electrical alternans pacing protocol—HVMs were preconditioned by pacing the LV endocardial apex at a cycle length (CL) of 1000ms for 20beats with 5ms long stimuli at twice capture amplitude. The LV apex was then dynamically paced with CL=550ms, and shortened by 50ms decrements until loss of 1:1 capture or reentry. Each pacing CL lasted for 32 beats since stable electrical alternans occurred after 20–24 beats for all CLs.

APV-ALT and CaT-ALT analyses—APV-ALT was analyzed using spectral methods for each CL's last 8 beats in the electrical alternans pacing protocol[1]. APV-ALT in the failing HVM was recorded when absolute voltage alternation (V_{alt}) was >twice the maximum control HVM V_{alt} with pacing CL=1000ms. CaT-ALT was analyzed by modifying the APV-ALT spectral method to compute absolute CaT alternation (C_{alt}),

$$C_{alt}=\sqrt{\frac{\sum T}{CaT\ duration}} \quad (1)$$

CaT duration was computed according to Lou et al[7], but at 90% recovery. Spectral magnitude was computed at 0.5 cycles/beat (ΣT) from peak CaT to 90% recovery. CaT-ALT in the failing HVM was recorded when C_{alt} was >twice the maximum control HVM C_{alt} with pacing CL=1000ms. Since ΣT is computed over the entire CaT, C_{alt} takes into account changes in both CaT peak amplitude and duration.

Discordant RT-ALT analysis—Spatial ventricular repolarization maps (*Rmap*) were computed for each CL's last 8 beats in the electrical alternans protocol,

$$Rmap(b,i)=AT(b,i)+APD_{90}(b,i) \quad i=0\rightarrow n \quad (2)$$

APD_{90} is APD at 90% repolarization, *i* the HVM node, *n* the total of HVM nodes, and *b* the beat number. The difference in subsequent *Rmaps* (*Rdiff*) was

$$Rdiff\,(b,i)=Rmap(b,i)-Rmap\,(b-1,i) \quad b=2\rightarrow 8 \quad (3)$$

Discordant RT-ALT was present at *i* when *Rdiff* magnitude was >1ms (temporal V_m resolution) and changed sign between subsequent beats. The gradient of each repolarization

map was computed ($\nabla Rmap(b,i)$) to quantify repolarization gradient steepening from discordant RT-ALT.

Discordant RT-ALT mechanisms were identified using published criteria[3,9]. Nodal lines for electrical alternans, $Rdiff(b,i)$=0, were calculated for each CL's last beat in the electrical alternans pacing protocol. When nodal lines approached the pacing site as CL shortened, discordant RT-ALT resulted from dynamically slowed conduction. When nodal line behavior was independent of the pacing site, discordant RT-ALT resulted from electrophysiological heterogeneities. To verify which mechanism, the alternans pacing protocol was executed with different pacing sites.

Electrical alternans spatial distribution—APV-ALT, CaT-ALT, and RT-ALT distributions were determined by subdividing the HVM into 4 regions (Figure 1) using the apicobasal direction (Φ_{ab}) and transmural (Φ_{tran}) directions defined in Supplementary Section 4. Apical and basal regions were defined as HVM nodes with Φ_{ab} values below and above the midpoint Φ_{ab} value, respectively. Endocardial and epicardial regions were defined as nodes with Φ_{tran} values below and above the midpoint Φ_{tran} value, respectively. For each region, the percentage of HVM nodes with electrical alternans was calculated for every CL.

HF parameter analysis—Each HF parameter in Supplementary Tables 2, 5, and 6 was switched to its control value, and the alternans pacing protocol and analyses repeated for each.

Comparisons with local clinical signals and complex APD oscillations—Local clinical signals were recorded as monophasic action potentials (MAPs). APV-ALT frequency spectra and complex APD oscillations in the HVM were computed from simulated MAPs to compare with their respective results in clinical MAPs (Supplementary Section 7).

Clinical

Patient recruitment—This study was approved by the joint Institutional Review Board of the Veterans Affairs and University of California Medical Centers, San Diego. All patients provided written informed consent. 53 *study* patients were recruited with LV ejection fraction (LVEF)<40% who underwent programmed stimulation prior to device implantation, and 18 *control* patients (LVEF>40%) undergoing ablation of supraventricular tachycardia (Supplementary Table 7). Excluded were patients with prior sustained VT/VF or aborted cardiac arrest within 30 days of an acute coronary syndrome or 6 weeks of revascularization, decompensated HF, or permanent pacemakers (to eliminate repolarization memory). Different from our prior studies[1,2] we analyzed prospectively acquired APV-ALT during *ventricular* pacing to more closely approximate *in silico* experiments, and analyzed the relationship of APV-ALT and complex APD oscillations to long-term follow-up.

Pacing—Patients underwent electrophysiology study in the post-absorptive state. A 7F MAP catheter (EP Technologies, Sunnyvale, CA) was advanced transvenously to the RV apex (n=62), or retrograde across the aortic valve to the LV (n=9) with heparin anticoagulation. Pacing commenced for 90sec with CL=500–600ms to record MAPs for

APV-ALT measurements. MAPs were filtered at 0.05–500Hz, digitized at 1kHz on a physiologic recorder (Bard, Billerica, MA), and analyzed offline.

APV-ALT and complex APD oscillation analyses—Clinical APV-ALT and complex APD oscillation analyses were analogous to the computational study. APV-ALT was quantified using the k-score to account for noise[1]. Complex APD oscillations and mean absolute ΔAPD were quantified for the last 10 paced beats at each CL (500–600ms) using customized Labview™(Austin, TX) software[10]. The optimal cutpoint of ΔAPD was defined to predict long-term VT/VF in a training sample (first half) of study patients. From receiver operating characteristics this was ≥2.3% of mean APD (Supplementary Figure 5).

Clinical Follow-up and Statistical Analyses—Patients were followed regularly with no loss to follow-up for the primary endpoint of appropriate implantable cardioverter defibrillator therapy or death. Continuous data was presented as mean+standard deviation, and compared in patients with dysfunctional and preserved LV using the two-tailed *t*-test. Paired continuous variables were compared using the paired, two-tailed *t*-test. The χ^2 test was applied to contingency tables of APV-ALT and complex APD oscillations against outcome. Kaplan-Meier curves of survival based on electrical alternans indices were constructed for the LV dysfunction patients. McNemar's test was used to compare predictive values of APV-ALT vs. complex APD oscillations. Significance was assessed at a two-tailed 0.05 alpha level.

Results

APV-ALT and CaT-ALT in the HVM and patients

APV-ALT and CaT-ALT were analyzed in nonfailing (control) and failing HVM during pacing. In the control HVM, APV-ALT and CaT-ALT were detected only at pacing CL<300ms, and arrhythmia did not occur prior to loss of 1:1 capture. In the failing HVM, APV-ALT and CaT-ALT were detected at the shorter pacing CL threshold of 550ms, leading to VT/VF at CL<400ms (Figure 1).

APV-ALT analysis results during pacing in patients paralleled HVM predictions. In 53 LV dysfunction patients, 26 reached the primary endpoint of VT/VF on extended follow-up of 48 months having greater APV-ALT than those whose did not (k-score 4.4±4.9 vs 1.1±3.0; p=0.036). ROC analysis on the training sample (n=26) showed APV-ALT k-scores>1.7 optimally predicted the primary endpoint (75% sensitivity, 78% specificity). In a test population (n=27), Kaplan-Meier analysis showed this cut-off separated primary endpoint patients (p<0.001; Supplementary Figure 6). Table 1 contains patient cohort repolarization dynamics.

APV-ALT transition to RT-ALT in the failing HVM

In the failing HVM, APV-ALT developed first with pacing CL≤550ms in the electrical alternans pacing protocol, transitioning into RT-ALT at CL 500ms (Figure 1). The amount of tissue with RT-ALT as a function of CL is shown for the apicobasal and transmural regions in Figure 1. Overall, RT-ALT did not develop homogeneously throughout the myocardium.

The failing HVM base was more susceptible to RT-ALT than the apex, and more so in the endocardium than epicardium.

Rate-dependent action potential and CaT dynamics were examined in the HVM endocardial apex and base to determine RT-ALT mechanisms. Figure 2 demonstrates the largest RT-ALT in the HVM base resulted from large APD_{90} and CaT peak amplitude alternans, not from action potential and CaT activation alternans. Note, action potential and CaT activation slowed more at shorter CL in the base than the apex due to longer basal APD.

Restoring SR calcium handling abolishes electrical alternans in the failing HVM

When each HVM HF parameter was adjusted back to its control value (healthy myocardium), only restoring SR calcium uptake (V_{maxup} Supplementary Tables 4,5) abolished electrical alternans with CL≥400ms and shifted the VT/VF threshold to CL<350ms. Restoring tissue conductivities in the failing HVM to control values, which primarily increases transverse conductivity velocity (Supplementary Tables 2, 3), did not affect the pacing CL thresholds or magnitudes of electrical alternans in Figure 1.

Arrhythmogenic apicobasal RT-ALT in the failing HVM

Arrhythmia was initiated in the failing HVM when pacing CL was shortened from 400 to 350ms (Figure 1). Figure 3A reveals arrhythmogenesis after 9 paced beats with CL=350ms; reentry from unidirectional conduction block at the myocardial region with the steepest repolarization (189ms/mm). The self-sustained reentry resembled VF in the pseudo-ECG (Figure 3B). AT and APD were plotted at and adjacent to the area of conduction block for the 9 beats preceding VF (Figure 3C); the figure shows discordant RT-ALT resulted from large discordant APD alternans (>100ms), but not AT alternans, and from slowed conduction in the base, where APD was longest. In contrast, the control HVM did not undergo drastic apicobasal repolarization gradient steepening, nor unidirectional conduction block and reentry with CLs between 550–350ms.

Mechanisms of arrhythmogenic discordant RT-ALT in the failing HVM

To explain apicobasal repolarization gradient steepening prior to conduction block in Figure 3A, we examined conduction, nodal lines, and spatial repolarization gradients prior to VF onset for CLs 400 and 500ms. During endocardial LV apex pacing (Figure 4A), conduction slowing occurred basally for the longer CL=500ms, where APD is longest and the first discordant RT-ALT nodal lines occurred. For CL=400ms, conduction slowing occurred closer to the apex, increasing the density of nodal lines and steepening repolarization over a larger HVM region. For CL<400ms, nodal lines overlapped HVM regions with the most rapid APD change (apicobasal midline in Supplementary Section 6), resulting in conduction block and reentry (Figure 3A). Nearly identical results were observed for endocardial RV pacing approximately midway from apex to base (Figure 4B). Thus, discordant RT-ALT (based on nodal line movement) arose apicobasal conduction slowing from APD heterogeneities (APD basal>apical).

Complex APD oscillations in failing human ventricles: in vivo and in silico

In vivo, complex APD oscillations occurred simultaneously with APV-ALT at CL≥500ms and predicted VT/VF during long-term follow-up. Patients with complex APD oscillations (≥2.3%) were more likely to reach the primary endpoint ($p<0.01$). Complex oscillations magnitude trended higher in patients reaching the primary endpoint (2.8±1.7 vs. 1.9±1.2%, $p=0.07$).

Figure 5A shows complex APD oscillations in a 26 year old patient with cardiomyopathy (LVEF=24%). Pacing produced non-alternating APD periodicity, shown as a large broad peak in the frequency spectra at 0.2–0.35 cycles/beat that eclipses the significant alternans peak. APV-ALT k-score was 13.27 with complex APD oscillations of 5.1%. This young man experienced sudden cardiac arrest from VT/VF in follow-up, rescued by his internal cardioverter defibrillator.

Figure 5B shows a 72 year old patient with cardiomyopathy (LVEF=26%) with a modest APV-ALT k-score=1.78. However, the broad frequency peak from 0.3–0.45 cycles/beat (non-alternating) showed marked complex oscillations of 2.4%. This individual later experienced primary VT/VF that would have been missed by APV-ALT yet detected by analyzing complex APD oscillations.

Figure 5C shows a 61 year old male with cardiomyopathy (LVEF 25%). His spectrogram demonstrated no alternans peak (k-score=−1.02) or complex oscillations <2.3% (1.3%), and was VT/VF free during 4 year follow-up.

In silico, Figure 6 demonstrates complex APD oscillations to occur in MAPs near non-stationary nodal lines of discordant RT-ALT. Non-uniform complex APD oscillations in MAPs resulted from spatial movements in RT-ALT nodal lines. MAPs in predominately concordant RT-ALT regions did not exhibit complex APD oscillations, or broader frequencies of APV-ALT. These results echoed those observed in HF patients, where only the presence of complex APD oscillations broadened the spectrum of APV-ALT to <0.5cycles/beat.

Combined electrical alternans indices in HF patients

APV-ALT had 82% positive and 54% negative predictive values. Complex APD oscillations had 78% positive and 57% negative predictive values. APV-ALT and/or complex APD oscillations had combined 82% positive and 90% negative predictive values of the primary endpoint. Measuring complex APD oscillations as a surrogate for discordant RT-ALT improved the predictability of APV-ALT for VT/VF. The use of complex APD oscillations to predict arrhythmogenic discordant RT-ALTs improved the sensitivity of alternans indices to 96% (specificity 60%).

RT-ALT effects on the ECG in the failing HVM

The pseudo-ECG of the failing HVM had beat-to-beat alternans during apical pacing with CL=500ms, and complex oscillations with CL=400ms (Figure 7). This is consistent with RT-ALT behavior in Figure 4, where the number of nodal lines (e.g. spatial distribution of discordant RT-ALT) increased significantly from CL of 500ms to 400ms. For CL≥500ms,

when RT-ALT was small in magnitude and discordant over limited regions with less nodal lines (compare Figures 2 and 4), the pseudo-ECG had visible beat-to-beat alternans. During apical pacing with CL=400ms, RT-ALT was discordant over larger regions with more nodal lines (compare Figures 2 and 4), and the pseudo-ECG exhibited complex oscillations.

Discussion

Using a combined computational-clinical approach, we established a novel mechanistic relationship between APV-ALT, complex APD oscillations, and VT/VF in human HF. *In vivo*, complex APD oscillations were found to accompany APV-ALT that developed into VT/VF, and the presence of both improved sensitivity of electrical alternans indices to predict VT/VF to 96% (60% specificity). *In silico*, abnormal SR calcium handling from HF led to APV-ALT near-resting heart-rates, which transitioned into discordant RT-ALT at faster rates that steepened apicobasal repolarization gradients to initiate VF via conduction block and reentry. Restoring SR calcium handing in the failing HVM was antiarrhythmic by eliminating electrical alternans. Importantly, simulations demonstrated that non-stationary discordant RT-ALT manifested in MAPs as complex APD oscillations, and not as beat-to-beat APD alternans. This combined computational-clinical study is the first to mechanistically link APV-ALT and complex APD oscillations in HF patients to arrhythmogenic discordant RT-ALT at elevated rates, which has implications for the development of new physiologically-tailored, bioengineering-designed indices that may improve risk stratification of VT/VF.

Ex vivo optical imaging studies corroborate HVM results

Lou et al[11] showed that discordant APD alternans precedes arrhythmogenesis in failing human RV wedge preparations. Reentry developed when pacing with CL=335ms, which corroborates VF initiation in the failing HVM (CL≤350ms). In simulations and experiments, apicobasal propagation was blocked at locations with discordant RT-ALT. This agreement between both strongly supports apicobasal repolarization gradient steepening, via discordant RT-ALT, as the primary mechanism for arrhythmia initiation at elevated heart-rates in human HF.

APD being greater in the ventricular base than apex may explain why apicobasal propagation is most vulnerable to conduction block and reentry. This longer basal APD slows conduction from the apex to base, which increases the likelihood of discordant RT-ALT (Figures 2,4). To show discordant RT-ALT arises from apicobasal APD heterogeneity, and not altered conduction from fibrosis and Cx43 remodeling in HF, tissue conductivity was restored back to healthy myocardial values (Supplementary Tables 2, 3). This did not affect electrical alternans magnitude or pacing CLs at which alternans developed, which can be attributed to the preservation of longitudinal conduction velocity under failing conditions[8].

Improving SR calcium handling in human HF is antiarrhythmic

APV-ALT transitioning to RT-ALT is linked primarily to CaT-ALT from abnormal SR calcium handling. SR calcium handling dysfunction in human HF significantly lowers the

heart-rate threshold for APV-ALT and CaT-ALT[1,2]. We found the same effect on arrhythmogenic discordant RT-ALT. Targeting SR calcium handling protein expressions by gene therapy could eliminate electrical alternans and suppress dangerous arrhythmias in HF[12]. Cutler et al[13] showed that overexpressing SERCA2a in ventricular myocytes suppresses CaT-ALT. Therefore, increasing SR calcium uptake could shift the threshold for arrhythmogenic discordant RT-ALT to much faster heart-rates. Other studies suggest targeting RyR channel kinetics governing SR calcium release is the more important therapeutic target for eradicating malicious electrical alternans[14,15]. HVMs could help calibrate such therapies for individual patients, and facilitate the discovery of additional targets for eradicating arrhythmogenic electrical alternans.

Improving clinical indices

This study provides insight into designing noninvasive and invasive clinical indices to stratify risk of VT/VF. Interest in microvolt T-wave alternans to non-invasively predict VT/VF[16] has recently been diminished due to its lack of specificity. Past studies report a strong relationship between T-wave heterogeneity and heightened VF propensity[17], where complex T-wave oscillations are believed to be linked to increased levels of spatial repolarization heterogeneity. We found complex ECG oscillations to be the result of arrhythmogenic discordant RT-ALT. Specifically, in the pseudo-ECG of the failing HVM, complex oscillations in the pseudo-ECG reflect the movement of discordant RT-ALT nodal lines (Figure 7). Future studies should investigate how to optimize discordant RT-ALT detection in the ECG T-wave to improve non-invasive risk stratification measurements as microvolt T-wave alternans.

Patient-specific modeling may also help improve VT /VF risk stratification in HF patients, similar to the approaches undertaken for patients with ischemic cardiomyopathy[18]. For example, spatial repolarization patterns vary between human hearts[19], where patients with large spatial repolarization gradients may be more prone to arrhythmogenic RT-ALT. Thus, electrical alternans pacing protocols may have significantly different results depending on pre-existing repolarization gradients. Clinical indices for predicting VT/VF from electrical alternans could be improved when combined with patient-specific measurements of spatial repolarization heterogeneity measurements.

Limitations

In the computational study, the first limitation was that the failing HVM is constructed from *ex-vivo* MRI scans of a structurally-normal heart. Altered geometry in human HF from myocyte and/or organ hypertrophy could potentially influence electrical alternans distribution and CL thresholds. However, an increase in myocardial wall thickness would likely have little affect on study results since transmural APD gradients are diminished in HF[6]. Second, the HVM did not include the His-Purkinje network, which could potentially contribute to RT-ALT, but its effects should be minimal since pacing from multiple sites resulted in similar electrical alternans distributions. Third, the HVM's human ventricular myocyte model (Supplementary references 5 and 6) lacked complex CaT dynamics[20,21]. Since abnormal SR calcium handling is essential in arrhythmogenic electrical alternans of

the failing HVM, future work is necessary to ascertain the most important SR calcium handling components governing CaT-ALT in HF.

In the clinical study, the first limitation was that simultaneous multiple site recordings were not routinely performed. Second, few patients had LV MAPs reflecting the difficulties in enrolling patients requiring clinical LV access. Third, cardiac motion, respiratory artifact or baseline wander could affect analysis. However, MAPs were consistent in shape, and such artifacts should not alternate every other beat. Fourth, analysis of discordance by the presence of complex APD oscillations is less direct than spatial mapping with optical imaging, but such methods are toxic and not available clinically, and previous studies have established that complex APD oscillations[10,22] arising in the context of alternans are indices of discordant electrical alternans. Fifth, a larger patient cohort is needed to decisively conclude that complex APD oscillations are statistically greater in HF than control patients (Table 1 *p*-values). Sixth, our study population reflects the male predominance of the Veterans Affairs population.

Conclusion

This combined computational-clinical study revealed mechanisms linking APV-ALT and complex APD oscillations at near-resting heart-rates with increased VT/VF vulnerability in human HF. *In vivo*, complex APD oscillations accompanied APV-ALT that developed into VT/VF, and the presence of both improved sensitivity of electrical alternans indices to predict VT/VF. *In silico*, abnormal SR calcium handling from HF led to APV-ALT at heart-rates near-rest that transitioned to RT-ALT at faster rates to initiate VT/VF. Complex APD oscillations accompanied APV-ALT and resulted directly from non-stationary discordant RT-ALT. Restoring SR calcium handling in the failing HVM eradicated all electrical alternans and increased the heart-rate threshold for VT/VF. These findings can be used to develop more effective strategies for stratifying VT/VF risk in patients.

Supplementary Material

Refer to Web version on PubMed Central for supplementary material.

Acknowledgments

Funding Sources:

This research was supported in part by AHA (10PRE3650037) and the Whitaker International Program administered by IIE to JDB, and IHU LIRYC (ANR-10-IAHU-04) to JDB and EJV. SMN was funded from NIH grants R01-83359 and K24-103800, and NAT from the NIH Director's Pioneer Award (PD1-HL123271).

References

1. Narayan SM, Bayer JD, Lalani G, Trayanova NA. Action potential dynamics explain arrhythmic vulnerability in human heart failure: a clinical and modeling study implicating abnormal calcium handling. Am J Cardiol. 2008; 52:1782–1792.
2. Bayer JD, Narayan SM, Lalani GG, Trayanova NA. Rate-dependent action potential alternans in human heart failure implicates abnormal intracellular calcium handling. Heart Rhythm. 2010; 7:1093–1101. [PubMed: 20382266]

3. Hayashi H, Shiferaw Y, Sato D, Nihei M, Lin SF, Chen PS, Garfinkel A, Weiss JN, Qu Z. Dynamic origin of spatially discordant alternans in cardiac tissue. Biophys J. 2007; 92:448–460. [PubMed: 17071663]
4. Pastore JM, Girouard SD, Laurita KR, Akar FG, Rosenbaum DS. Mechanism linking T-wave alternans to the genesis of cardiac fibrillation. Circulation. 1999; 99:1385–1394. [PubMed: 10077525]
5. Watanabe MA, Fenton FH, Evans SJ, Hastings HM, Karma A. Mechanisms for discordant alternans. J Cardiovasc Electr. 2001; 12:196–206.
6. Glukhov AV, Fedorov VV, Lou Q, Ravikumar VK, Kalish PW, Schuessler RB, Moazami N, Efimov IR. Transmural dispersion of repolarization in failing and nonfailing human ventricle. Circ Res. 2010; 106:981–991. [PubMed: 20093630]
7. Lou Q, Fedorov VV, Glukhov AV, Moazami N, Fast VG, Efimov IR. Transmural heterogeneity and remodeling of ventricular excitation-contraction coupling in human heart failure. Circulation. 2011; 123:1881–1890. [PubMed: 21502574]
8. Glukhov AV, Fedorov VV, Kalish PW, Ravikumar VK, Lou Q, Janks D, Schuessler RB, Moazami N, Efimov IR. Conduction remodeling in human end-stage nonischemic left ventricular cardiomyopathy. Circulation. 2012; 125:1835–1847. [PubMed: 22412072]
9. Sato D, Shiferaw Y, Garfinkel A, Weiss JN, Qu Z, Karma A. Spatially discordant alternans in cardiac tissue: role of calcium cycling. Circ Res. 2006; 99:520–527. [PubMed: 16902177]
10. Narayan SM, Franz MR, Clopton P, Pruvot EJ, Krummen DE. Repolarization alternans reveals vulnerability to human atrial fibrillation. Circulation. 2011; 123:2922–2930. [PubMed: 21646498]
11. Lou Q, Janks DL, Holzem KM, Lang D, Onal B, Ambrosi CM, Fedorov VV, Wang IW, Efimov IR. Right ventricular arrhythmogenesis in failing human heart: the role of conduction and repolarization remodeling. Am J Physiol. 2012; 303:H1426–1434.
12. del Monte F, Harding SE, Schmidt U, Matsui T, Kang ZB, Dec GW, Gwathmey JK, Rosenzweig A, Hajjar RJ. Restoration of contractile function in isolated cardiomyocytes from failing human hearts by gene transfer of SERCA2a. Circulation. 1999; 100:2308–2311. [PubMed: 10587333]
13. Cutler MJ, Wan X, Laurita KR, Hajjar RJ, Rosenbaum DS. Targeted SERCA2a gene expression identifies molecular mechanism and therapeutic target for arrhythmogenic cardiac alternans. Circ Arrhythm Electrophysiol. 2009; 2:686–694. [PubMed: 19948504]
14. Picht E, DeSantiago J, Blatter LA, Bers DM. Cardiac alternans do not rely on diastolic sarcoplasmic reticulum calcium content fluctuations. Circ Res. 2006; 99:740–748. [PubMed: 16946134]
15. Wang L, Myles RC, De Jesus NM, Ohlendorf AK, Bers DM, Ripplinger CM. Optical mapping of sarcoplasmic reticulum Ca2+ in the intact heart: ryanodine receptor refractoriness during alternans and fibrillation. Circ Res. 2014; 114:1410–1421. [PubMed: 24568740]
16. Narayan SM. T-wave alternans and the susceptibility to ventricular arrhythmias. Am J Cardiol. 2006; 47:269–281.
17. Nearing BD, Verrier RL. Tracking cardiac electrical instability by computing interlead heterogeneity of T-wave morphology. J Appl Physiol. 2003; 95:2265–2272. [PubMed: 12897035]
18. Hermenegild A, Guallar E, Jebb A, Malamas P, Wu KC, Trayanova NA. Arrhythmia risk stratification of patients after myocardial infarction using personalized heart models. Nat Commun. 2016 In Press.
19. Opthof T, Janse MJ, Meijborg VM, Cinca J, Rosen MR, Coronel R. Dispersion in ventricular repolarization in the human, canine and porcine heart. Prog Biophys Mol Biol. 2016; 120:222–235. [PubMed: 26790342]
20. O'Hara T, Virag L, Varro A, Rudy Y. Simulation of the undiseased human cardiac ventricular action potential: model formulation and experimental validation. PLoS Comput Biol. 2011; 7:e1002061. [PubMed: 21637795]
21. Grandi E, Pasqualini FS, Bers DM. A novel computational model of the human ventricular action potential and Ca transient. J Mol Cell Cardiol. 2010; 48:112–121. [PubMed: 19835882]
22. Nearing BD, Verrier RL. Progressive increases in complexity of T-wave oscillations herald ischemia-induced ventricular fibrillation. Circ Res. 2002; 91:727–732. [PubMed: 12386150]

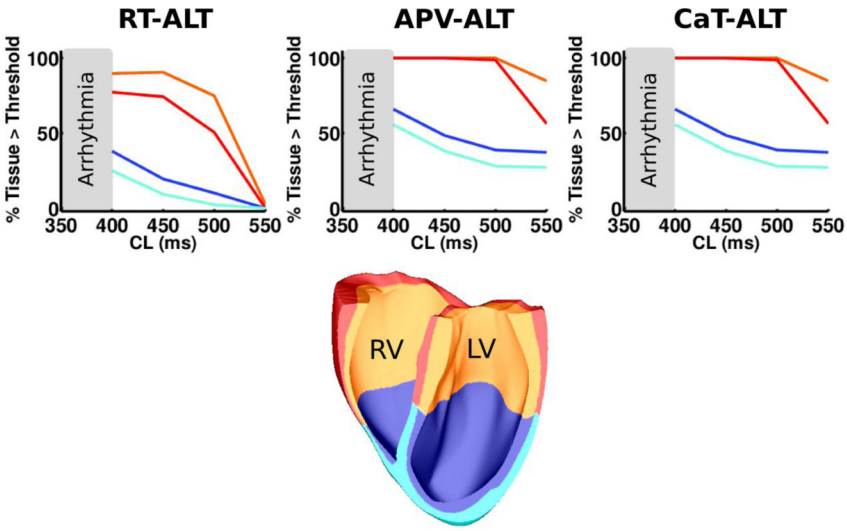

Figure 1.

Rate-dependent distribution of alternans in the failing HVM colored according to their respective HVM location (orange=basal endocardium, red=basal epicardium, blue=apical endocardium, cyan=apical epicardium).

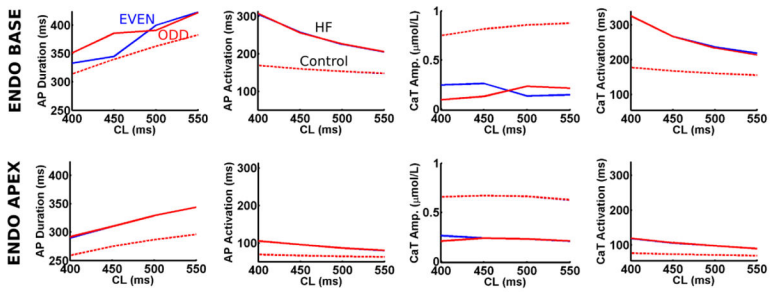

Figure 2. Action potential (AP) and calcium transient (CaT) dynamics underlying RT-ALT in the failing HVM

Odd (red) and even (blue) beats for AP and CaT duration and activation sampled from the endocardial apex and base. Control HVM traces are plotted with dashed lines.

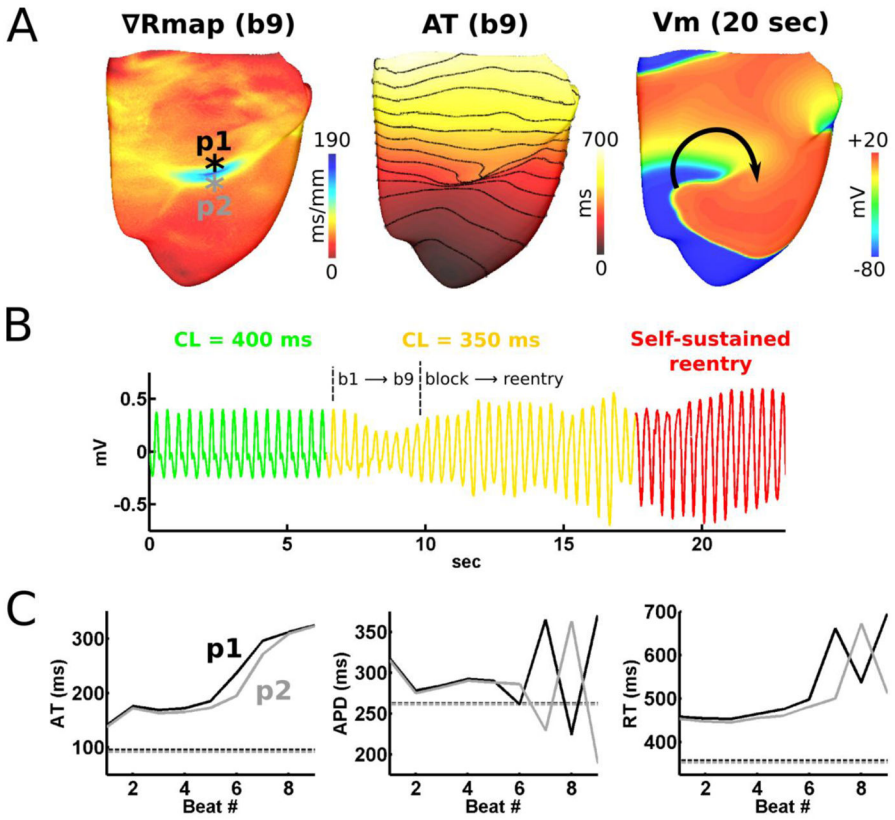

Figure 3. Arrhythmogenesis in the failing HVM

(A) Repolarization, activation (50ms isochrone line spacing), and transmembrane voltage (V_m) maps corresponding to (B), the pseudo-ECG resembling VF in precordial lead V1. (C) APD, activation time (AT), and repolarization time (RT) at the highlighted location in (A) for the 9 beats prior arrhythmia initiation.

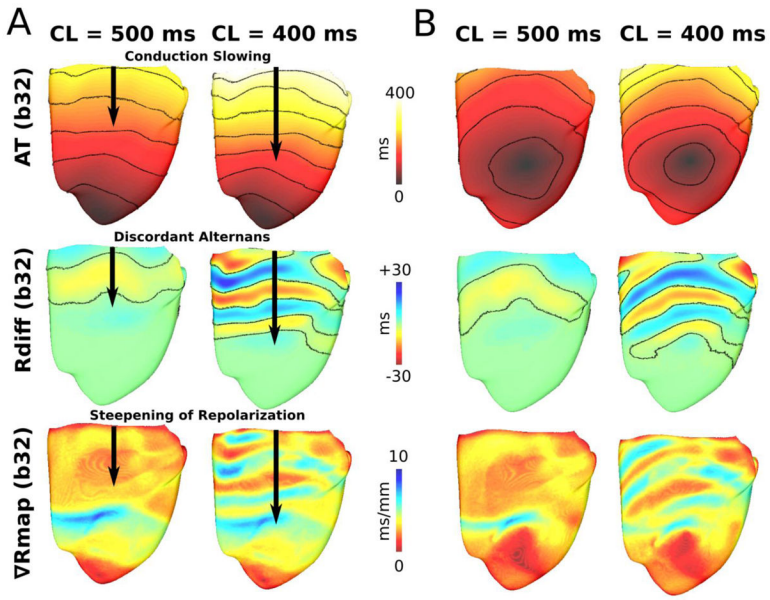

Figure 4. Discordant RT-ALT in the failing HVM

Activation (50ms isochrone lines spacing), *Rdiff*, and *Rmap* maps revealing apicobasal rate-dependent conduction slowing, discordant RT-ALT, and steepening of repolarization, respectively, during endocardial LV apex (A) and epicardial RV (B) pacing.

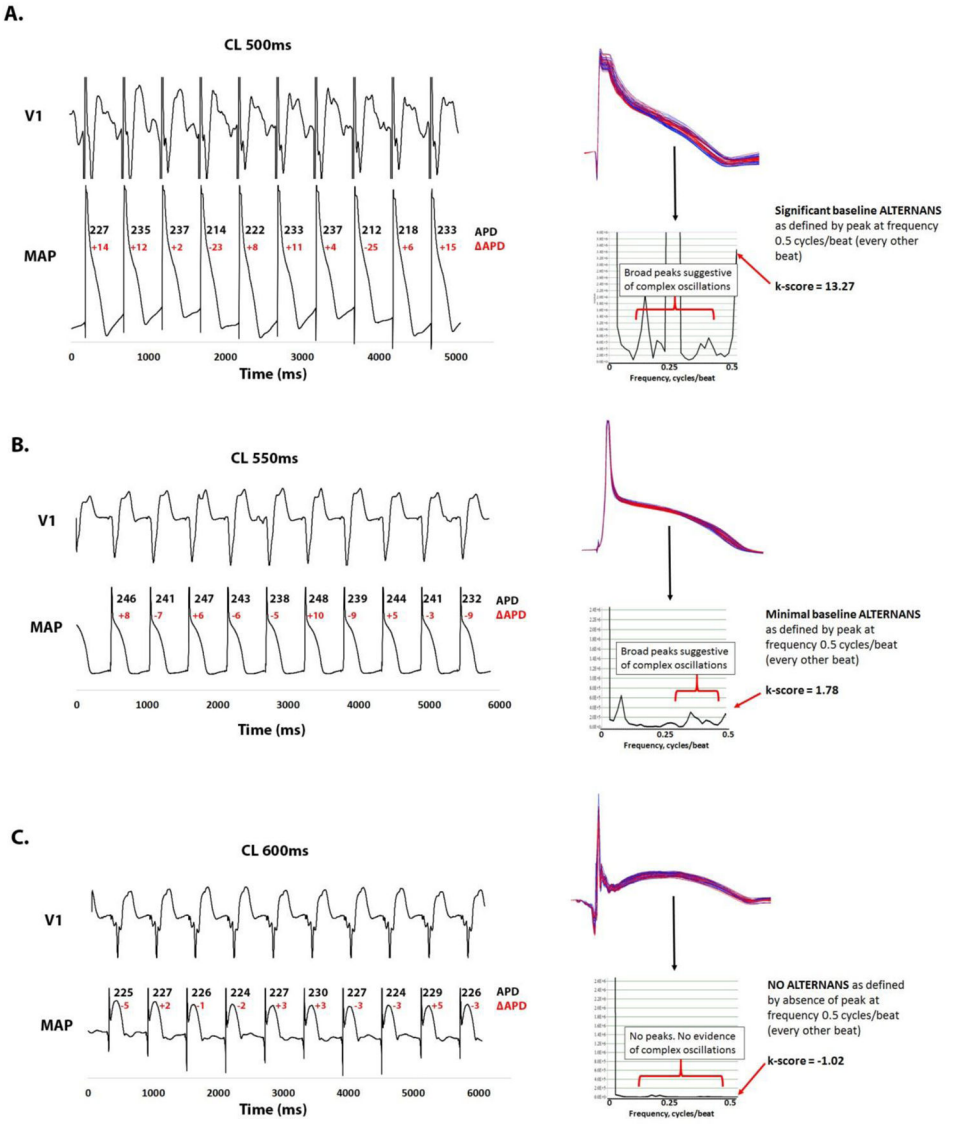

Figure 5. Complex APD oscillations and APV-ALT predict VT/VF in HF patients

(A) 26 year old male with cardiomyopathy and VT/VF on follow-up showing complex, non-alternating, APD oscillations constituting 5.1% of mean APD during pacing with CL=600ms. The frequency spectrum showed a broad peak at 0.2–0.35 cycles/beat (non-alternating periodicity) even greater than the significant alternans peak at 0.5 cycles/beat (k-score>13.27). (B) 72 year old male with cardiomyopathy and VT/VF during follow-up showing minimal complex APD oscillations (2.4%) and a broad peak at 0.3–0.45 cycles/beat, yet a modest alternans peak (k-score 1.78). (C) 61 year old male with cardiomyopathy and no events during follow-up free of complex APD oscillations (1.3%) and APV-ALT (k-score=−1.03).

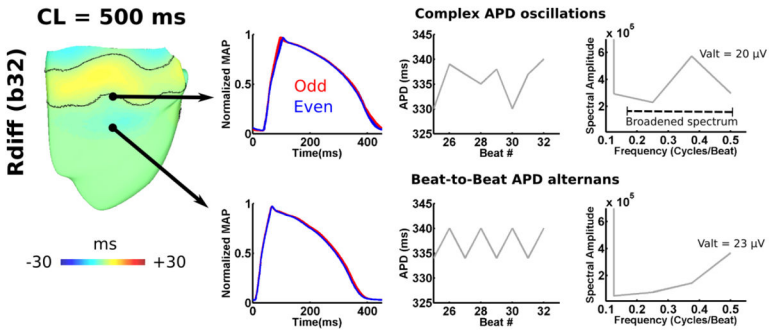

Figure 6. Complex APD oscillations in the failing HVM

For the *Rdiff(b32)* at the pacing CL=500ms, complex APD oscillations were detected only near RT-ALT nodal lines. As in HF patients, the presence of complex APD oscillations broadened spectral alternans frequency to <0.5 cycles/beat.

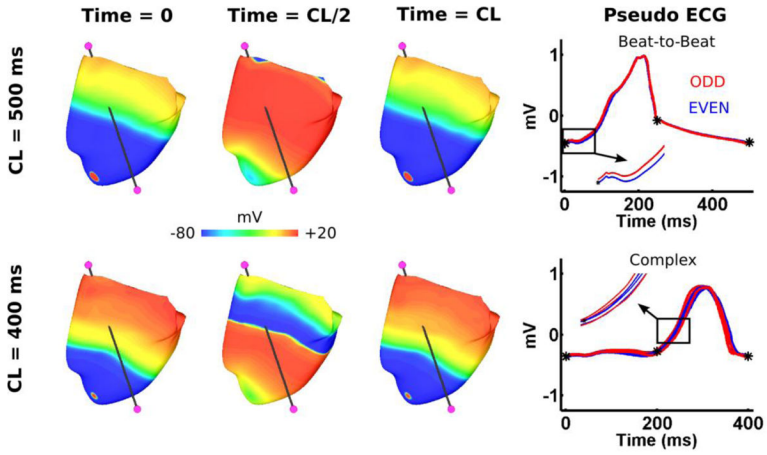

Figure 7. Pseudo-ECG for the failing HVM during apical pacing with CLs of 400 and 500ms

The pseudo-ECG was computed by taking the basal extracellular voltage subtracted from the apical extracellular voltage (electrodes in magenta). Beat-to-beat alternans and complex oscillations in the pseudo-ECGs are shown by superimposing the odd (Red) and even (Blue) beats during the last 8 of 32 beats for the two pacing CLs. Transmembrane voltage maps are shown for the HVM at three different time points for the first of the last 8 superimposed beats.

Table 1

Patient cohort repolarization dynamics with pacing CL=550ms

	LV Dysfunction (n=53)	Preserved LV (n=18)	p-value
APV-ALT			
k-score	2.8±4.4	0.7±3.3	0.06
k-score≥1.7,n(%)	18(34)	2(11)	0.06
Amplitude, μV	21.9±39.7	2.5±4.6	0.06
APD ALTERNANS			
mean APD, ms	250±35	239±28	0.25
mean ΔAPD, ms	6.0±3.9	4.6±5.0	0.23
Complex APD Oscillations (%mean APD)	2.5±1.6	1.9±2.1	0.27
Complex APD Oscillations≥2.3%,n(%)	22(42)	5(28)	0.30
COMBINED ALTERNANS INDEX			
k-score≥1.7 OR Complex Oscillations≥2.3%,n(%)	32(60)	5(28)	**0.02**